Polymer 52 (2011) 3587–3596

Contents lists available at ScienceDirect

Polymer

journal homepage: www.elsevier.com/locate/polymer

Novel approach toward poly(butylene succinate)/single-walled carbon nanotubes nanocomposites with interfacial-induced crystallization behaviors and mechanical strength

Licheng Tan [a,b], Yiwang Chen [a,b,*], Weihua Zhou [a,*], Suwen Ye [a], Junchao Wei [b]

[a] Institute of Polymers, Nanchang University, 999 Xuefu Avenue, Nanchang 330031, PR China
[b] Department of Chemistry, Nanchang University, 999 Xuefu Avenue, Nanchang 330031, PR China

ARTICLE INFO

Article history:
Received 25 February 2011
Received in revised form
2 June 2011
Accepted 4 June 2011
Available online 12 June 2011

Keywords:
Single-walled carbon nanotube
Nanocomposites
Crystallization

ABSTRACT

Biodegradable poly(butylene succinate) (PBS)/single-walled carbon nanotube (SWCNT) nanocomposites were successfully prepared through silication and physical blend between PBS and acyl aminopropyltriethoxysilane functionalized single-walled carbon nanotube (SWCNT-APTES), which was obtained from acylate between 3-aminopropyltriethoxysilane and acyl chloride functionalized single-walled carbon nanotube. Fourier transform infrared spectroscopy (FTIR) and nuclear magnetic resonance (NMR) observations revealed that the PBS chains were covalently attached to the SWCNT-APTES by hydrolysis. PBS/SWCNT-APTES nanocomposites after hydrolysis exhibited strong interfacial interaction between SWCNT-APTES and PBS matrix, leading to a less agglomeration. However, the PBS/SWCNT-APTES nanocomposite prepared by only physical blend without hydrolysis exhibited severe reagglomeration of SWCNT in the PBS. The addition of SWCNT-APTES enhanced the crystallization of the PBS in the nanocomposites for both approaches of hydrolysis and physical blend due to the heterogeneous nucleation effect while the crystal structure of PBS remained. Especially, a more significant increase of crystallization rate for physical blend was present as comparison to PBS/SWCNT-APTES after hydrolysis due to the higher diffusion constant, which is attributed to the change of surface properties of nanotubes. Furthermore, the incorporation of SWCNT-APTES improved the storage modulus of the nanocomposites compared with that of neat PBS. The PBS/SWCNT-APTES nanocomposites after hydrolysis showed of higher tensile strength than PBS/SWCNT-APTES nanocomposite without hydrolysis.

1. Introduction

Increasing demand for special materials has led to the conception of composites, since valuable properties of different types of materials can be combined [1]. Nowadays, numerous nanomaterials such as clays, carbon nanotubes and cellulose nanowhiskers, are presently considered to be high-potential filler materials for the improvement of thermal, electrical and mechanical properties of polymers, which have recently gained considerable interests in both the academic and industrial fields [2–8].

Carbon nanotubes (CNTs) have been considered as ideal reinforcing fillers for polymer matrixes to achieve high performance and multifunctions, because of their nanometer size, high aspect ratios, and more importantly, their extraordinary mechanical strength and high electrical and thermal conductivity [9–11]. Some biodegradable polymers/CNTs nanocomposites have recently been studied, including chitosan, poly(lactic acid), polycaprolactone and poly(butylene succinate) etc [7–21].

Poly(butylene succinate) (PBS) is a biodegradable aliphatic polyester and commercially available as thermoplastic polyester with many interesting properties, including biodegradability, melt processability, thermal and chemical resistance. However, some properties of PBS, such as softness, weak gas barrier and slow biodegradation rate, are frequently insufficient for various end-use applications. Incorporation with inorganic or organic fillers is an effective approach for improving the physical/chemical properties of PBS and other biopolymers. Recently, Pramoda et al. prepared poly(butylene succinate) (PBS)/multi-walled carbon nanotubes (MWCNTs) nanocomposites by melt

* Corresponding authors. Nanchang University, Institute of Polymers, 999 Xuefu Avenue, Nanchang 330031, PR China. Tel.: +86 791 3969562; fax: +86 791 3969561.
E-mail addresses: ywchen@ncu.edu.cn (Y. Chen), dramzwh@126.com (W. Zhou).

0032-3861/$ – see front matter © 2011 Elsevier Ltd. All rights reserved.
doi:10.1016/j.polymer.2011.06.006

compounding and studied the effect of MWCNT dispersion on the modulus and crystallization kinetics [22]. Qiu et al. also prepared PBS/MWCNTs nanocomposites by solution blending at 1 wt% MWCNTs [23].

However, to obtain the uniform dispersion of carbon nanotubes in the polymer matrix is very difficult due to the insolubility of the carbon nanotubes and the inherently poor compatibility between the carbon nanotubes and the polymer, and the resulting inhomogeneous nanocomposites often have unsatisfying properties. For the direct blending of CNTs and polymers, carbon nanotubes tend to aggregate, and their nonuniform dispersion in the polymer matrix often results in deleterious effects. Chemical bonding of polymeric matrix with CNTs will greatly enhance their combinations [24].

Consequently, some methods must be proposed for functionalizing the carbon nanotubes before using them as the fillers in the polymer matrix [25]. One of these is an oxidative process utilizing strong acids, such as HNO_3 or H_2SO_4, by which hydroxyl and carboxylic acid moieties are created on nanotubes [26]. The silanization of functionalized nanotubes is another preferred method used to enhance the interfacial adhesion between nanotubes and the matrix. 3-Aminopropyltriethoxysilane (3-APTES) is an important aminosilane that finds wide applications in nylon, phenolic, epoxy, and melamine resin based composites [27].

To the best of our knowledge, SWCNT modified by APTES in PBS nanocomposites have never been reported. In this study, biodegradable poly(butylene succinate) (PBS)/single-walled carbon nanotube (SWCNT) nanocomposites were successfully prepared through silication and physical blend between PBS and acyl aminopropyltriethoxysilane functionalized single-walled carbon nanotube (SWCNT-APTES). Furthermore, the effect of interfacial interactions produced from covalent bonding and physical blend between PBS and SWCNT-APTES on the dispersion of SWCNT in the PBS matrix, crystallization behavior and mechanical properties of the PBS/SWCNT-APTES nanocomposites was studied in detail with various techniques.

2. Experimental

2.1. Materials

Poly(butylene succinate) (PBS) used in this study was synthesized by the two-stage melt polycondensation from dimethyl succinate (DMS) and 1,4-butanediol (BDO) in the presence of titanium (IV) butoxide ($Ti(OBu)_4$) catalyst at 180 °C for 2 h and followed 230 °C for 6 h under nitrogen atmosphere and reduced pressure with vigorous stirring according to the previous work [28]. The single-walled carbon nanotubes (SWCNTs) were purchased from Chengdu Organic Chemicals Co. Ltd., Chinese Academy of Sciences (purity >95%, length: 10–20 μm, outside diameter: 20–30 nm, inside diameter: 10–20 nm). Dimethyl succinate (DMS) was purchased from Alfa Aesar Co., Ltd (Tianjin, China). 1,4-butanediol (BDO) was purchased from Sinopharm Chemical Reagent Co., Ltd (Shanghai, China). 3-Aminopropyltriethoxysilane with purity of 99% (Aldrich) was used as the silane coupling agent. The reagents were used as received without further purification. Titanium (IV) butoxide ($Ti(OBu)_4$) catalyst was purchased from Acros. All the other chemicals and solvents of analytical grade were used as received without further purification.

2.2. Functionalization of SWCNTs

The surface modification of SWCNTs was achieved as shown in Scheme 1. 3.0 g of pristine SWCNTs were dispersed in 300 ml of concentrated H_2SO_4/HNO_3 (3:2 v/v) solution in an ultrasonic bath (40 kHz) for 30 min, and refluxed under magnetic stirring for 20 h at 50 °C. Next, the dispersion was diluted in water, vacuum-filtered and washed with deionized water several times until a pH of approximately 7.0 was reached. The sample was then dried in vacuum at 40 °C overnight, resulting in SWCNTs modified with carboxyl groups (SWCNT–COOH). A suspension of 1.0 g of SWCNT–COOH in 100 ml of $SOCl_2$ was placed in a 250 ml round bottom flask and refluxed for 24 h under a dry air atmosphere.

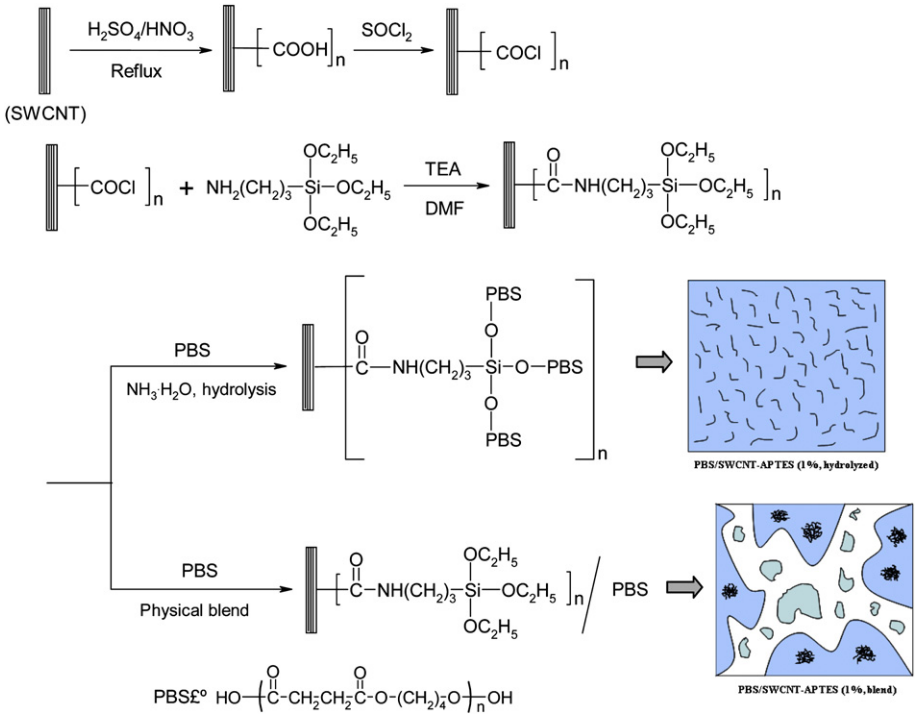

Scheme 1. Synthesis of PBS/SWCNT-APTES nanocomposites.

Surplus $SOCl_2$ was removed directly from the system by vacuum distillation, avoiding chloride-induced damaged to the SWCNTs. The reaction mixture was then cooled to room temperature, with the result being SWCNTs functionalized with acyl chloride groups (SWCNT–COCl). Next, 0.3 g SWCNT–COCl was reacted with 15 ml of APTES in 50 ml of N,N′-dimethyl formamide (DMF) under a dry air atmosphere at 120 °C for 24 h. A few drops of triethylamine were added as phase transfer catalyst. After reaction, the excess solvent was removed by vacuum distillation, and the resulting black solid was washed by dehydrated DMF and ethanol repeatedly and then dried in vacuum at room temperature for 24 h, giving acyl aminopropyltriethoxysilane functionalized single-walled carbon nanotube (SWCNT-APTES).

2.3. Preparation of PBS/SWCNT-APTES nanocomposites

PBS/SWCNT-APTES nanocomposites were prepared by physical blend and hydrolysis, respectively (Scheme 1). 10 mg SWCNT-APTES was dispersed in 40 mL DMF and sonicated in an ultrasonic bath for 30 min to achieve uniform dispersion. Next, 1.0 g PBS was added into SWCNT-APTES suspension and sonicated for another 10 min to dissolve PBS completely. The mixture solution was sonicated at 80 °C for 3 h, and then precipitated into an excess of methanol, collected on a filter. Finally, the PBS/SWCNT-APTES (1%, blend) nanocomposite was dried at 40 °C for 24 h under vacuum. For preparation of PBS/SWCNT-APTES (1%, hydrolyzed) nanocomposite with 1 wt% of SWCNT-APTES in PBS matrix, ammonia was added dropwisely to mixture of SWCNT-APTES and PBS in DMF with stirring at 80 °C for 3 h. By hydrolysis, PBS was covalently attached onto SWCNT. The mixture was precipitated into an excess of methanol, collected on a filter and dried under vacuum at 80 °C for 24 h. The thin films sandwiched between two polyamides films were prepared by MY-8200-10 Hot Press. The samples were heated at 150 °C for 3 min to erase the thermal history. Subsequently, the films with the thickness of about 0.15 mm were obtained by cooling to room temperature. The films were cut into a sheet of 22 × 5 mm and used for the mechanical testing. The received films were also used directly for XRD and DMA characterization. The films were fractured by the treatment of liquid nitrogen, and used for the observation by SEM. The samples using for AFM observation were prepared by spin-coating sample solutions onto silicon substrates at 1000 rpm. The samples using for TEM observation were also prepared by spin-coating sample solutions onto silicon substrates at 1000 rpm, and the films were taken out and used for TEM analysis.

2.4. Measurements

Fourier transform infrared spectroscopy (FTIR) spectra for samples were recorded in a manner of KBr tablet on a Shimadzu IRPrestige-21 FTIR spectrophotometer. All FTIR spectra were collected under the room temperature over a scanning range of 400–4000 cm^{-1}. Nuclear magnetic resonance (NMR) spectra were collected on a Bruker AV 600 NMR spectrometer with deuterated $CDCl_3$ as the solvent and with tetramethylsilane ($\delta = 0$) as the internal standard.

The fracture surfaces of samples obtained by the liquid nitrogen treatment were observed with Quanta 200F scanning electron microscopy (SEM) after gold vapor deposition onto the samples in an Edwards Auto 306. The morphologies of PBS/SWCNT-APTES nanocomposites were characterized with a JEM-2010 (HR) transmission electron microscope (TEM). The TEM was operated at 100 kV and was also used to obtain the crystal structure of the products by selected area electron diffraction (SAED). Atomic force microscopy (AFM) images of pure PBS and PBS/CNT-APTES nanocomposites sheets were taken in the tapping mode by carrying out on SPA-400.

Thermogravimetric analysis (TGA) was performed on a PerkinElmer TGA 7 at a heating rate of 20 °C/min under nitrogen with a sample size of 8–10 mg. Differential scanning calorimetry (DSC) measurements of copolyesters were carried out on a Shimadzu DSC-60 under a nitrogen flow. The calibration of the temperature was performed using indium as the standard before the measurement. For nonisothermal crystallization, about 5 ± 0.1 mg of samples encapsulated in the DSC aluminum pan, were first heated to 150 °C at 30 °C/min and held for 5 min to erase thermal history. Then, the samples were cooled to −50 °C and subsequently heated to 150 °C at 10 °C/min. The corresponding glass transition temperature (T_g), melting temperature (T_m), crystallization temperature (T_c), melting enthalpy (ΔH_m) and crystallization enthalpy (ΔH_c) were recorded, respectively. For isothermal crystallization, the samples were annealed at 150 °C for 5 min to eliminate thermal history, cooled to the crystallization temperature (T_c) at cooling rate of 100 °C/min, and the maintained at T_c until the crystallization was completed. The exothermal traces were recorded for the later data analysis.

Wide-angle X-ray diffraction patterns (WAXD) measurements of the samples were performed by a Bruker D8 Focus X-ray diffractometer, operating at 30 kV and 20 mA with a copper target ($\lambda = 0.154$ nm) and in the 2θ angle range of 5–40° at a scanning rate of 0.5°/min. The crystal morphology of the copolyesters was analyzed by a Nikon E600POL polarizing optical microscope (POM) equipped with an Instec HS 400 heating and cooling stage.

Mechanical properties of the copolyesters were determined by a SANS WDW universal test system with electronic data evaluation on specimen of 70 × 25 mm with a thickness in the range of 0.04–0.06 mm determined by a vernier caliper. The specimens were cut from melt-pressed films by a mold equipped with knives. The values of tensile strength, elongation at break and tensile modulus were determined. Data were taken as the average value of at least five measurements. Dynamic mechanical properties of pure PBS and PBS/CNT-APTES nanocomposites were measured with a dynamic mechanical analyzer (DMA, Perkin–ElmerQ800) for rectangular samples of about 0.1 mm in thickness using the tensile mode at a constant frequency of 1 Hz and a heating rate of 3 °C/min scanning from −80 to 80 °C.

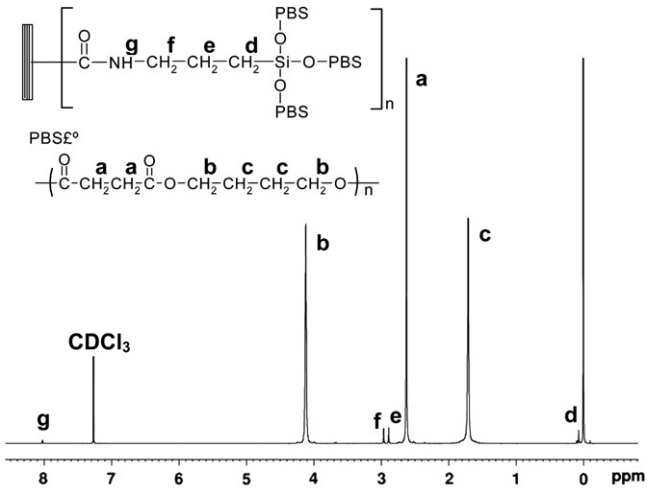

Fig. 1. 600 MHz ^1H NMR spectrum of the PBS/SWCNT-APTES (1%, hydrolyzed) nanocomposite.

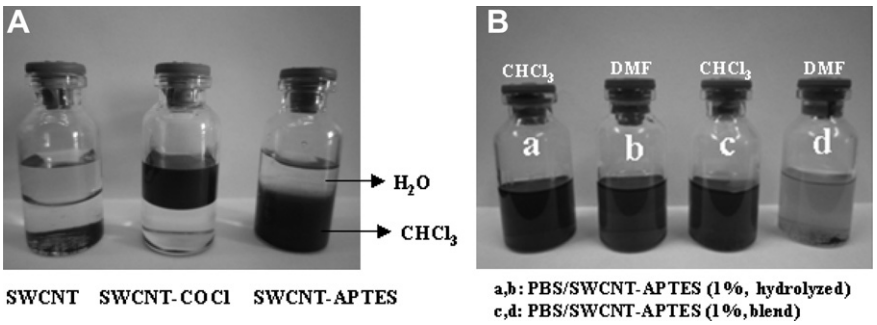

Fig. 2. Dispersion of (A) SWCNT, SWCNT–COCl, and SWCNT-APTES in water/chloroform solution and (B) PBS/SWCNT-APTES nanocomposites in chloroform and N, N-Dimethyl formamide.

3. Results and discussion

3.1. Characterization of PBS/SWCNT-APTES nanocomposites

In order to prove that the PBS chains were successfully covalent bonding with SWCNT-APTES by hydrolysis, the product of PBS/SWCNT-APTES (1%, hydrolyzed) nanocomposite was washed thoroughly with chloroform and filtered to remove any chloroform-soluble substances such as the PBS unbound to the SWCNT. Washing was continued until no polymer could be detected in the filtrate.

FTIR spectrum (see Supporting information) of pristine SWCNT exhibited typical C=C stretching bands at 1530 cm^{-1}, which corresponds to the graphene structure of SWCNT [29]. In the spectrum of SWCNT-APTES, the broad band around 3430 cm^{-1} is assigned to the hydrogen-bonded amide group of APTES, whereas the bands between 1532 and 1650 cm^{-1} are assigned to the combination of bending of the N–H bond and stretching of the C–N bond in the amide group. C–H stretching vibrations also occur around 2950 cm^{-1}. Signals corresponding to C–N and Si–O stretches can be seen at 1087 and 1019 cm^{-1}, respectively [30,31]. Additionally, SWCNT-APTES displayed a weak carbonyl (C=O) stretching band at 1710 cm^{-1}. For PBS/SWCNT-APTES (1%, hydrolyzed), more intense C=O stretching band appeared at 1720 cm^{-1}. The difference in C=O stretching band positions between SWCNT-APTES and PBS/SWCNT-APTES attributes to the fact that the band at 1710 cm^{-1} of SWCNT-APTES is due to the acyl chloride groups and the band at 1720 cm^{-1} of PBS/SWCNT-APTES is owing to the ester groups of covalent bonded PBS chains. The peaks at 2950–2850 cm^{-1} also become more prominent and are ascribed to C–H stretching of CH_2 hydrocarbon chains of covalent bonded PBS.

Fig. 1 illustrates the ^1H NMR spectra of PBS/SWCNT-APTES (1%, hydrolyzed) after washing with chloroform to remove the unbound PBS completely. The peak at 2.67 ppm (proton **a**), 4.12 ppm (proton **b**) and 1.71 ppm (proton **c**) are assigned to protons from the CH_2 protons of PBS, respectively. The peak at 0.07 ppm (proton **d**), 2.89 ppm (proton **e**) and 2.96 ppm (proton **f**) are ascribed to different CH_2 of SWNT-APTES. Furthermore, the peak at 8.02 ppm (proton **g**) is assigned to the N*H* of APTES. These results reveal that the PBS chains were successfully covalently attached to SWCNT-APTES by hydrolysis.

Fig. 2 shows the hydrophilicity and hydrophobicity of different samples in the absence of pristine SWCNT. However, the dispersion of SWCNT–COCl and SWCNT-APTES was remarkably changed after modification. SWCNT–COCl is hydrophilic and well dispersed in water, whereas SWCNT-APTES, with the silane coupling agents, is hydrophobic and disperses well in chloroform. Besides, PBS/SWCNT-APTES (1%, hydrolyzed) is more stable than PBS/SWCNT-APTES (1%, blend) in DMF solution. It is revealed that the PBS molecular chains have been incorporated onto the surfaces of SWCNT-APTES via silanization in the presence ammonia. Therefore, the incorporated PBS chains onto the surface of carbon nanotubes significantly improve the stability in DMF due to the good solubility of PBS in DMF. The difference in dispersion of PBS/SWCNT-APTES in DMF is mainly due to the surface modification of SWCNT-APTES by PBS.

3.2. Morphology of PBS/SWCNT-APTES nanocomposites

The dispersion of SWCNTs in polymer is one of the most important topics for fabricating high performance polymer/SWCNTs composites. With respect to neat PBS, the PBS/SWCNT-

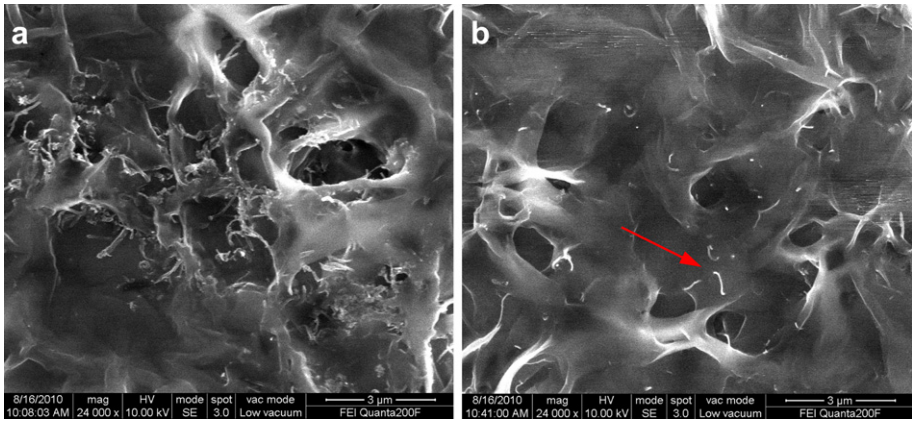

Fig. 3. Representative SEM images of nanocomposites: (a) PBS/SWCNT-APTES (1%, blend) and (b) PBS/SWCNT-APTES (1%, hydrolyzed), respectively.

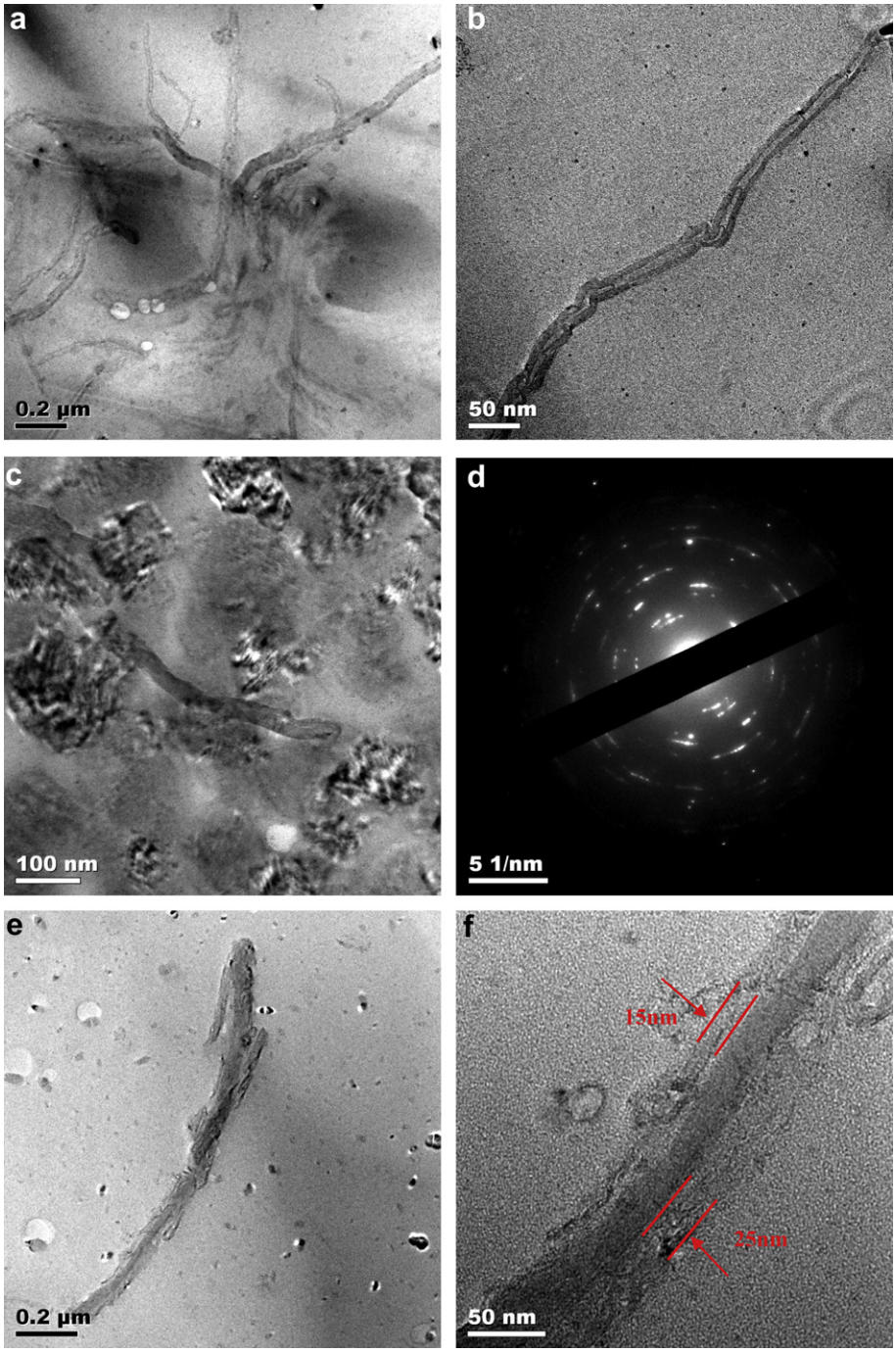

Fig. 4. TEM images of (a, b, c, d) PBS/SWCNT-APTES (1%, blend) and (e, f) PBS/SWCNT-APTES (1%, hydrolyzed).

APTES nanocomposite after hydrolysis showed of strong interfacial interactions between SWCNTs and polymer matrix, thus the dispersion of the nanotubes could be improved. The good dispersing of SWCNT-APTES and the strong interfacial interaction between PBS and SWCNT-APTES may eventually affect the thermal and mechanical properties of the nanocomposites [32]. To reveal the dispersion of SWCNT-APTES in the PBS matrix, the fracture surfaces and ultrathin section of the nanocomposites were investigated in detail by SEM, TEM and AFM, respectively.

Fig. 3 shows the SEM images of the PBS/SWCNT-APTES (1%, blend) and PBS/SWCNT-APTES (1%, hydrolyzed) nanocomposite. The random dispersed bright dots and lines are the ends of the broken carbon nanotubes. For the PBS/SWCNT-APTES (1%, blend) nanocomposite, severe aggregation of SWCNT-APTES is observed in Fig. 3a. It is seen from Fig. 3b that the individual SWCNT-APTES are randomly dispersed in PBS/SWCNT-APTES (1%, hydrolyzed) nanocomposite, and no apparent SWCNT aggregation is observed. The results indicate that the morphology of PBS/SWCNT-APTES (1%, hydrolyzed) nanocomposite is different from the PBS/SWCNT-APTES (1%, blend) nanocomposite, attributing to the good dispersion of SWCNT-APTES in PBS matrix and the stronger interfacial interactions between PBS and SWCNT-APTES by covalent bonding.

The dispersion of PBS/SWCNT-APTES nanocomposites was further analyzed by TEM (Fig. 4). In the TEM images of PBS/SWCNT-APTES

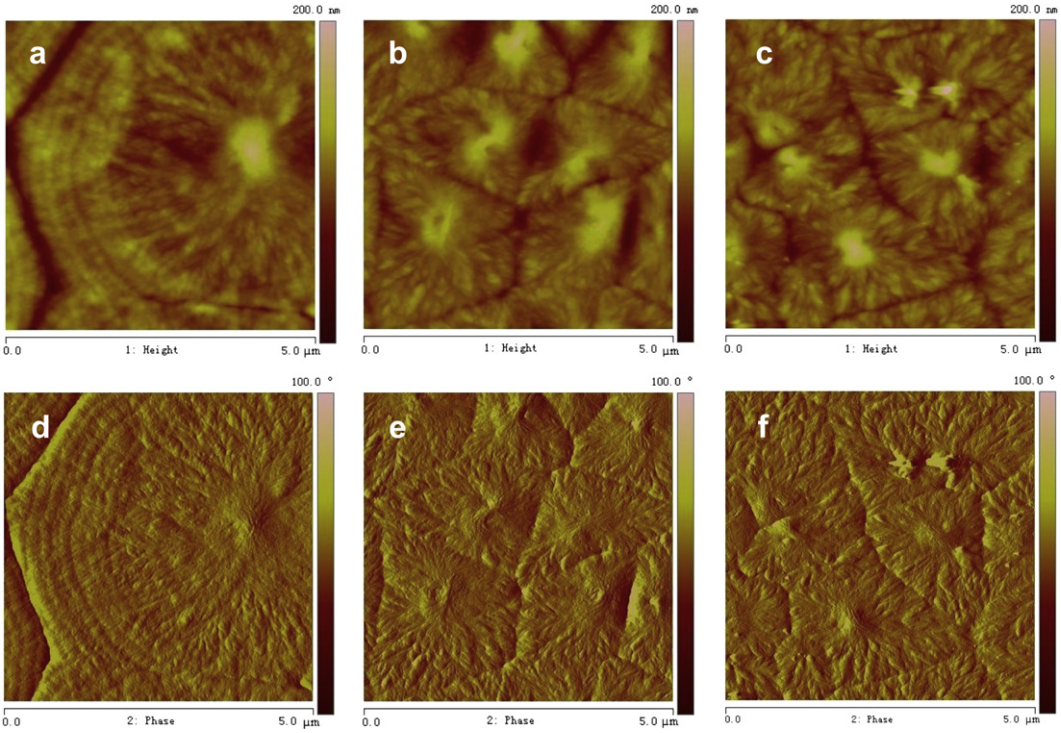

Fig. 5. AFM height and phase images (5 μm × 5 μm) of nanocomposites: (a, d) PBS (b, e), PBS/SWCNT-APTES (1%, hydrolyzed) and (c, f) PBS/SWCNT-APTES (1%, blend).

(1%, blend) nanocomposite, the SWCNT-APTES wall is relatively smooth and clear without any extra phase adhering to it. From the SAED pattern, it could be seen that the circumjacent regions around SWCNT-APTES show of the crystalline phase of PBS. In contrast, the PBS/SWCNT-APTES (1%, hydrolyzed) nanocomposite (Fig. 4e–f) show an obvious core-shell structure with the polymer layer as the shell and SWCNT-APTES at the center, the thickness of the PBS shell is about 15–25 nm. It is obvious that SWCNT-APTES is homogeneously dispersed in the PBS/SWCNT-APTES (1%, hydrolyzed) nanocomposite without any apparent aggregation. The nanostructures and morphology of the PBS/SWCNT-APTES nanocomposites have also been analyzed by AFM. Fig. 5 shows the AFM height and phase images of neat PBS and PBS/SWCNT-APTES nanocomposites. In the AFM height image of Fig. 5a–c, surface of neat PBS film is smooth, whereas that of the nanocomposite films show dark and bright contrasts, which are corresponding to the low and high regions, respectively. From the AFM phase images (Fig. 5d–f), the apparent PBS spherulite patterns were observed. The diameter of the spherulites decreases as the incorporation of SWCNT-APTES, which is similar to the later POM analysis.

3.3. Thermal stability and crystallization of PBS/SWCNT-APTES nanocomposites

Fig. 6 shows the typical TGA curves of SWCNT-APTES, PBS and PBS/SWCNT-APTES nanocomposites. The decomposition temperature (T_d) at 5% weight loss is around 333 °C for neat PBS and increases to be around 340–347 °C for the nanocomposites. It is clear that the thermal stability of PBS is improved by an increase of about 10 °C after the incorporation of functionalized SWCNT-APTES. Table 1 shows the decomposition temperatures (T_d) at 5% weight loss for all the nanocomposites. The PBS/SWCNT-APTES (1%, hydrolyzed) nanocomposite shows a relatively higher stability than PBS/SWCNT-APTES (1%, blend), due to the formation of covalent bonding between PBS and SWCNT-APTES after hydrolysis, showing of better dispersion in the PBS matrix.

Fig. 7 shows the DSC cooling and heating curves for PBS and PBS/SWCNT-APTES nanocomposites. Table 1 provides a summary of the DSC results, including of the glass transition temperature (T_g), melting temperature (T_m), crystallization temperature (T_c), melting enthalpy (ΔH_m) and crystallization enthalpy (ΔH_c), respectively. The crystallization temperature of all the nanocomposites were higher than that of neat PBS, and increased with the increase of the nanotube content, indicating that the SWCNTs served as the nucleating agent and promoted the crystallization rate of PBS. As compared with the PBS/SWCNT-APTES (1%,

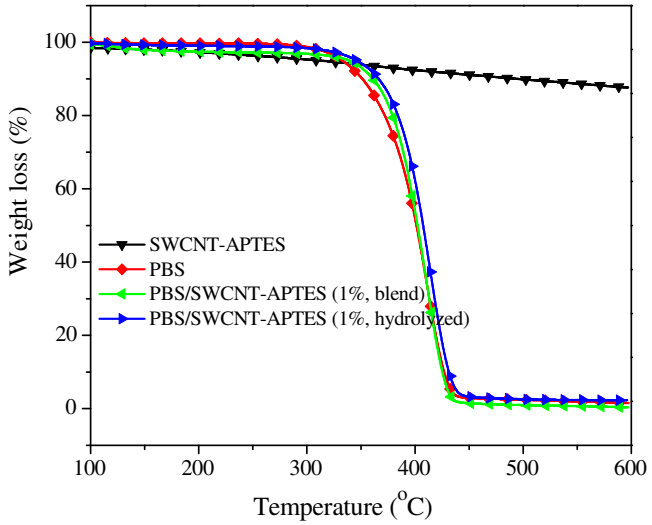

Fig. 6. TGA curves of SWCNT-APTES, neat PBS, PBS/SWCNT-APTES (1%, hydrolyzed) and PBS/SWCNT-APTES (1%, blend).

Table 1
Thermal properties of neat PBS and its nanocomposites.

Sample	T_g (°C)	T_m (°C)	ΔH_m (J/g)	T_c (°C)	ΔH_c (J/g)	T_d (°C)
PBS	−28.6	110.8	71.2	73.5	63.6	332.7
PBS/SWCNT-APTES (0.5%, hydrolyzed)	−27.5	111.2	53.8	81.3	62.4	339.1
PBS/SWCNT-APTES (1%, hydrolyzed)	−26.2	111.3	55.6	81.5	61.4	343.7
PBS/SWCNT-APTES (2%, hydrolyzed)	−25.3	111.0	62.1	85.1	65.6	344.6
PBS/SWCNT-APTES (3%, hydrolyzed)	−24.8	111.2	62.4	86.7	67.2	346.5
PBS/SWCNT-APTES (1%, blend)	−27.0	111.5	61.4	86.0	63.2	340.2

Glass transition temperature (T_g), melting temperature (T_m), crystallization temperature (T_c), crystallization enthalpy (ΔH_c) and melting enthalpy (ΔH_m) were registered by DSC at a cooling rate of 10 °C/min or at a second heating rate of 10 °C/min. Thermal decomposition temperature (T_d) (−5 wt%) was measured by TGA at a heating rate of 20 °C/min.

hydrolyzed) nanocomposites, double crystallization peaks with some overlap were observed for PBS/SWCNT-APTES (1%, blend). This is due to the fact that the agglomeration was so bad that some PBS chains which were so far away from a nanotube surface that it crystallizes at the same rate that pure PBS crystallizes at causing the two peaks. Moreover, two T_ms were found for all nanocomposites in the heating thermograms. The most likely explanation could be related to formation of crystals with different thickness. The crystal with thin lamellae melts at relatively lower temperature, and the crystal with thick lamellae melts at higher temperature, leading to the appearance of double melting peaks. The temperature of the first T_m for the nanocomposites was much higher than that of neat PBS. As the PBS/SWCNT-APTES (1%, hydrolyzed) nanocomposites are concerned, the relative intensity of melting peak at low temperature becomes stronger by the increase of SWCNT-APTES. It is revealed that the existence of SWCNT-APTES induced more content of imperfect crystals as compared with pristine PBS. However, the PBS/SWCNT-APTES (1%, blend) nanocomposite exhibits the stronger melting peak at low temperature than PBS/SWCNT-APTES (1%, hydrolyzed) nanocomposites, which is probably due to the fact that the SWCNT-APTES (1%, blend) induced the nucleation of PBS and the formation of crystals with thin thickness during the crystallization process. The PBS/SWCNT-APTES (1%, blend) nanocomposite shows more ratio of first melting enthalpy in the two enthalpies, due to the formation of more content of imperfect crystals. Most probably, they are connected with a minute fraction of thinner and/or less perfect crystals formed during the quenching of the films to room temperature after cold crystallization [33]. The temperature of the second T_m for the nanocomposites was similar to that of PBS and more probable to refer to the melting temperature of the originally crystallized parts.

The overall isothermal melt crystallization kinetics of neat PBS and the PBS/SWCNT-APTES nanocomposites was investigated by DSC in a wide range of crystallization temperatures (T_cs). According to the Avrami equation, the relative degree of crystallinity (X_t) develops as a function of crystallization time t as follows:

$$1 - X_t = \exp(-kt^n) \quad (1)$$

where X_t is the relative crystallinity at time t, k is the crystallization rate constant, and n is the Avrami exponent depending on the nature of nucleation and growth geometry of the crystals [34]. In order to deal conveniently with the operation, Eq. (1) is usually rewritten as a double logarithmic from as follows:

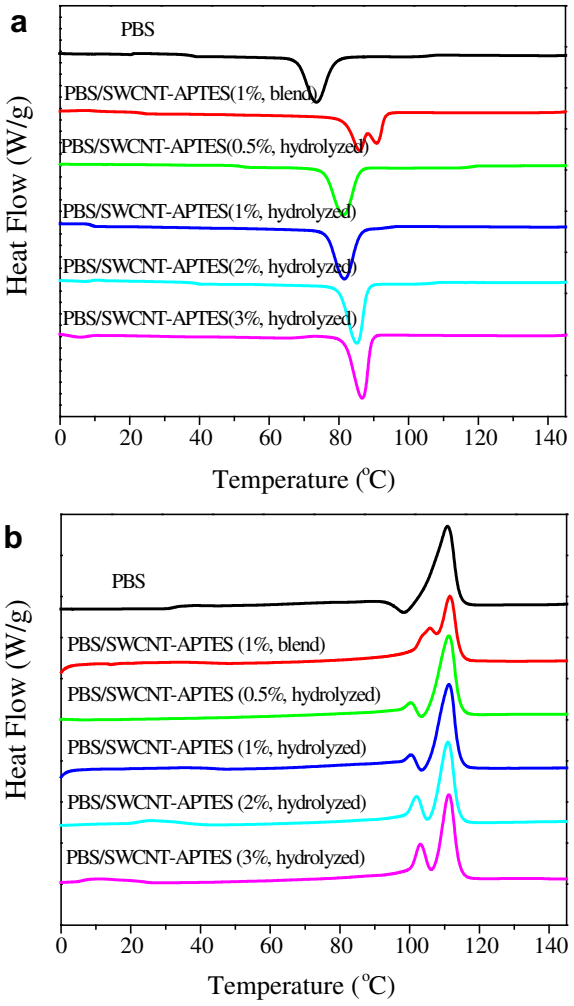

Fig. 7. DSC thermograms of neat PBS and its nanocomposites: (a) cooling and (b) second heating curves.

$$\ln[-\ln(1 - X_t)] = \ln k + n \ln t \quad (2)$$

The relative degree of crystallinity as a function of the time and the Avrami plots of $\ln[-\ln(1-X_t)]$ versus $\ln t$ for PBS and the PBS/SWCNT-APTES nanocomposites at various T_cs could see in Supporting information. The Avrami parameters n and k obtained from the slopes and intercepts of the Avrami plots are summarized in Table 2, from which it can be seen that the average values of n are varied between 2.5 and 2.8 for both PBS and the nanocomposites at the indicated T_cs. The slight variation in the n values indicates that the interfacial interactions between PBS and SWCNT-APTES may not change the crystallization mechanism of PBS in the PBS/SWCNT-APTES nanocomposites. However, it should be noted that it is difficult to compare the overall crystallization rate directly from the values of n and k because n is not constant and the unit of k is min^{-n}. Thus, the half-time of crystallization $t_{0.5}$, the time required to achieve 50% of the final crystallinity of the samples, is introduced for the discussion of crystallization kinetics. The value of $t_{0.5}$ is calculated by the following equation:

$$t_{0.5} = \left(\frac{\ln 2}{k}\right)^{1/n} \quad (3)$$

Accordingly, the values of $t_{0.5}$ and $1/t_{0.5}$ are listed in Table 2. With increasing of T_c, the $1/t_{0.5}$ values decrease while $t_{0.5}$ values

Table 2
Summary of isothermal crystallization kinetics of neat PBS and its nanocomposites at different crystallization temperatures.

Sample	T_c (°C)	n	k (min^{-n})	$t_{0.5}$ (min)	$1/t_{0.5}$ (min^{-1})
PBS	82	2.8	2.51×10^{-1}	1.44	0.70
	84	2.9	9.18×10^{-2}	2.01	0.50
	86	2.8	4.12×10^{-2}	2.74	0.37
	88	2.8	8.96×10^{-3}	4.73	0.21
PBS/SWCNT-APTES	88	2.8	8.41×10^{-1}	0.93	1.07
(1%, hydrolyzed)	90	2.8	3.40×10^{-1}	1.30	0.97
	92	2.9	6.50×10^{-2}	2.26	0.44
	94	3.0	1.23×10^{-2}	3.83	0.26
PBS/SWCNT-APTES	90	2.6	2.53	0.61	1.65
(3%, hydrolyzed)	92	2.8	1.14	0.84	1.20
	94	2.9	2.92×10^{-1}	1.33	0.75
	96	2.9	6.68×10^{-2}	2.24	0.45
PBS/SWCNT-APTES	94	2.4	7.54	0.37	2.70
(1%, blend)	96	2.6	2.27	0.63	1.58
	98	2.6	5.90×10^{-1}	1.07	0.94
	100	2.4	1.94×10^{-1}	1.70	0.59

increase for both PBS and the nanocomposites. Such variations indicate that the overall isothermal crystallization rate decrease with the increase of T_c due to the low supercooling in the chosen crystallization temperature range. The $1/t_{0.5}$ values are lager in the PBS/SWCNT-APTES nanocomposites than in neat PBS at a given T_c, indicating that heterogeneous nucleation effect of SWCNT for PBS.

In addition, $1/t_{0.5}$ value of PBS/SWCNT-APTES (1%, hydrolyzed) nanocomposite after hydrolysis is lower than PBS/SWCNT-APTES (1%, blend) nanocomposite, showing that the crystallization rate depressed after hydrolysis. This result is unique due to the better dispersion of carbon nanotubes in PBS/SWCNT-APTES (1%, hydrolyzed) nanocomposite. In the PBS/SWCNT-APTES (1%, blend) nanocomposite, the severe agglomeration of carbon nanotubes was observed. And the reagglomeration does not increase crystallization rate, the rate increases initially with better dispersion. At high nanotube contents, a decrease can occur, but this is due to the reduction in growth due to diffusion constant reductions. In this case, the grafting is more important than the dispersion since the more poorly dispersed sample without grafting has a higher rate. During the crystallization process, the existence of carbon nanotubes served as the nucleating agent, leading to the crystallization of PBS at higher temperatures. After hydrolysis, the PBS molecular chains were linked onto the surfaces of carbon nanotubes, and the interfaces between carbon nanotubes and PBS were changed. Thus, the nucleation rate of the PBS should be affected. Furthermore, the PBS molecular chains incorporated onto the surfaces of carbon nanotubes become less flexible, and the diffusion of PBS chains onto the crystallization growth front is difficult, leading to the reduction of crystal growth rate. Therefore, the crystallization rate was reduced by the diffusion constant reductions.

Fig. 8 shows the spherulites of neat PBS and its nanocompostites. It can be seen that the size of PBS spherulites becomes smaller in the presence of SWCNT-APTES, indicative of stronger heterogeneous nucleation effect of SWCNT-APTES. Some smaller and imperfect spherulites are observed in the nanocomposites, which grow rapidly, impinge quickly with surrounding spherulites and restrict further growth. SWCNT-APTES can be clearly seen as black dots. On the basis of the POM results, it can be concluded that the nucleation density of PBS in its nanocomposites could be enhanced by the presence of SWCNT-APTES. The results are consistent with those obtained by AFM and DSC analysis. In this study, the effect of the addition of SWCNT-APTES on the crystal structure of PBS was studied by WAXD (see Supporting information). It is also noticed that the nanocomposites exhibit the similar reflection peaks as those of neat PBS, showing that the incorporating of SWCNT-APTES does not change the crystal structure of PBS.

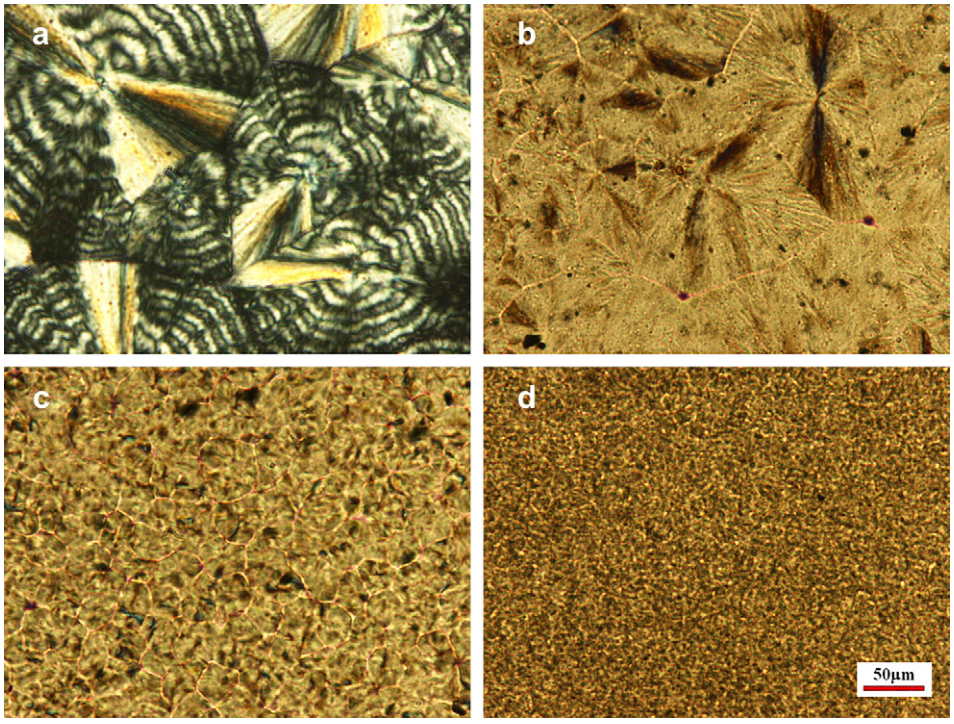

Fig. 8. POM graphs for PBS and its nanocomposites of (a) PBS crystallized at 80 °C, (b) PBS/SWCNT-APTES (0.5%, hydrolyzed) crystallized at 88 °C, (c) PBS/SWCNT-APTES (1%, hydrolyzed) crystallized at 90 °C, and (d) PBS/SWCNT-APTES (1%, blend) crystallized at 94 °C, respectively. The scale is the same for all photographs.

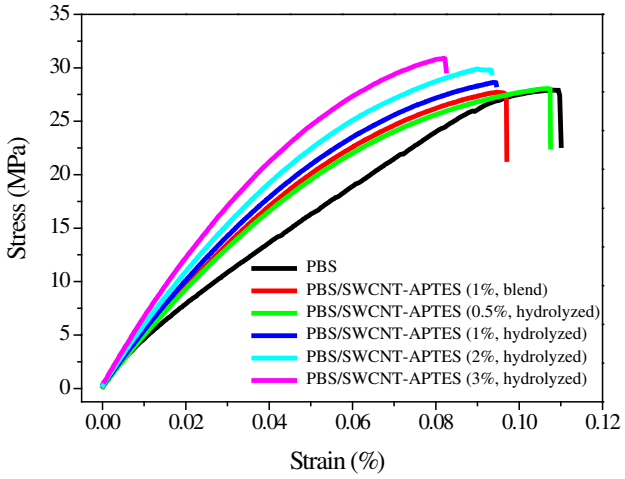

Fig. 9. Stress–strain curves of neat PBS and its nanocomposites.

3.4. Mechanical properties of PBS/SWCNT-APTES nanocomposites

The typical stress–strain curves of PBS and PBS/SWCNT-APTES nanocomposites are shown in Fig. 9 and the corresponding results are listed in Table 3. It is noted that the addition of SWCNT-APTES significantly enhances the elastic modulus of PBS due to the incorporation of rigid components into the relatively soft PBS matrix. In addition, the tensile strength of PBS increases slightly with the increase of SWCNT-APTES content. As compared with the PBS/SWCNT-APTES (1%, blend) nanocomposite, the PBS/SWCNT-APTES (1%, hydrolyzed) nanocomposite shows of higher tensile strength, due to the better dispersion of SWCNT-APTES in PBS matrix after hydrolysis. However, the elongation at break of the nanocomposites is lower than neat PBS, which is attributed to the reduced flexibility of PBS chains in the nanocomposites by the addition of SWCNT-APTES.

Fig. 10 shows the storage modulus (E′) and loss tangent (tan δ) versus temperature for PBS and its nanocomposites. It is observed that the neat PBS exhibits the E′ value of 3020 MPa at −50 °C. By increase of the SWCNT-APTES content to 3 wt%, the E′ value reaches to 4460 MPa, showing that the storage modulus of PBS was significantly improved by the addition of SWCNT-APTES. Furthermore, the E′ value of PBS/SWCNT-APTES (1%, blend) nanocomposite is lower than that of PBS/SWCNT-APTES (1%, hydrolyzed) nanocomposite, indicating of good dispersion of SWCNTs in PBS matrix after hydrolysis. Accordingly, as observed from Fig. 10b, it is observed that the glass transition temperatures remain in the same region between −50 °C and 40 °C upon incorporating of SWCNT-APTES into PBS matrix. However, a slight increase in T_g could still

Table 3
Mechanical properties of neat PBS and its nanocomposites.

Sample	Tensile Strength (MPa)	Elongation at break (%)	Elastic Modulus (MPa)
PBS	26.4 ± 1.5	12.9 ± 0.5	401.2 ± 35.6
PBS/SWCNT-APTES (0.5%, hydrolyzed)	27.1 ± 0.9	11.3 ± 0.8	482.5 ± 14.6
PBS/SWCNT-APTES (1%, hydrolyzed)	28.6 ± 1.1	9.8 ± 1.2	513.0 ± 33.0
PBS/SWCNT-APTES (2%, hydrolyzed)	29.5 ± 1.3	9.3 ± 0.4	570.7 ± 32.5
PBS/SWCNT-APTES (3%, hydrolyzed)	30.6 ± 2.0	8.0 ± 0.7	626.4 ± 28.1
PBS/SWCNT-APTES (1%, blend)	26.9 ± 1.6	10.4 ± 1.1	485.3 ± 20.7

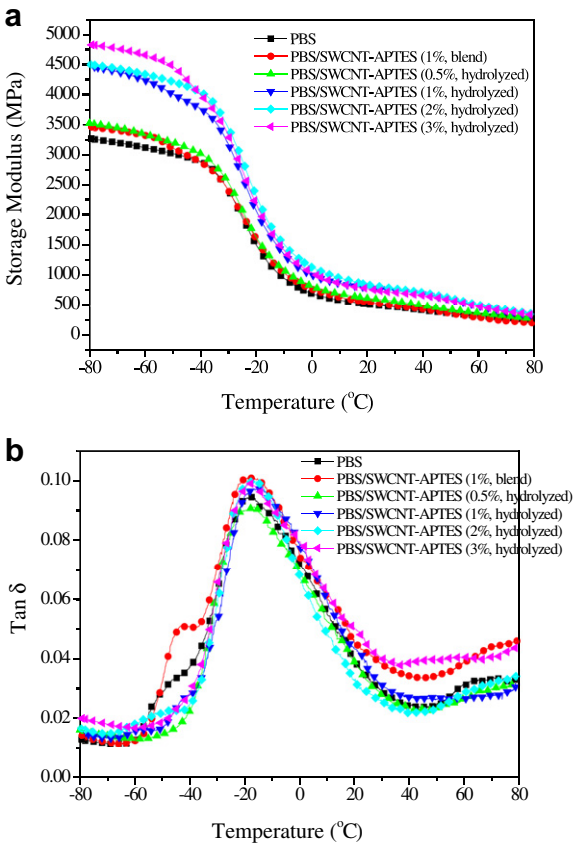

Fig. 10. Temperature dependence storage modulus and tan δ curves of neat PBS and its nanocomposites.

be observed with the increase of SWCNT-APTES content, showing that the incorporation of SWCNT-APTES restricted the molecular movement of PBS. In the lower temperature region, one more distinct peak at the temperature of −43 °C is visible for PBS/SWCNT-APTES (1%, blend) nanocomposites. The other samples do not exhibit the obvious peak similar to that of the PBS/SWCNT-APTES (1%, blend) nanocomposite. This could be related to the change of the interfacial interactions between PBS and carbon nanotubes. For the PBS/SWCNT-APTES (1%, blend) nanocomposite, there should be physical interactions between the PBS matrix and surfaces of carbon nanotubes. The secondary relaxation of PBS near the surfaces of SWCNT-APTES might be induced by the interfacial interactions. For the PBS/SWCNT-APTES nanocomposites after hydrolysis, the PBS molecular chains were chemically linked to the surfaces of carbon nanotubes. Therefore, the secondary relaxation of PBS was not observed due to the change of the interfacial properties. Based on the DSC results, the T_g of PBS increased with the increase of SWCNT-APTES content, showing that the movement of PBS molecular chains was restricted by the carbon nanotubes. Furthermore, the T_g in PBS/SWCNT-APTES (1%, hydrolyzed) is higher than that in PBS/SWCNT-APTES (1%, blend), showing of better dispersion of SWCNT in PBS matrix after hydrolysis.

4. Conclusions

Biodegradable poly(butylene succinate) (PBS)/single-walled carbon nanotube (SWCNT) nanocomposites were successfully prepared through covalent bonding and physical blend between PBS and acyl aminopropyltriethoxysilane functionalized SWCNT (SWCNT-APTES). The FTIR and NMR spectra revealed that the PBS

chains were covalently attached to the SWCNT-APTES by hydrolysis. The incorporation of SWCNT-APTES enhanced the crystallization of the PBS in the nanocomposites due to the heterogeneous nucleation effect. Covalent bonding after hydrolysis forced SWCNT with better dispersion in the PBS matrix and nanocomposites with higher tensile strength and less loss tan δ. The crystallization rate of PBS/SWCNT-APTES (1%, blend) nanocomposite was higher than PBS/SWCNT-APTES (1%, hydrolyzed) nanocomposite, which is might be due to the reduction of growth constant after hydrolysis.

Acknowledgments

Financial support for this work was provided by the Natural Science Foundation of Jiangxi Province (2009GQH0068), and Program for Innovative Research Team in University of Jiangxi Province.

Appendix. Supporting information

Supplementary data associated with this article can be found, in the online version, at doi:10.1016/j.polymer.2011.06.006.

References

[1] Njuguna J, Pielichowski K, Desai S. Polym Adv Technol 2008;19(8):947–59.
[2] Kelarakis A, Giannelis EP. Polymer 2011;52(10):2221–7.
[3] Mishra AK, Chattopadhyay S, Rajamohanan PR, Nando GB. Polymer 2011; 52(4):1071–83.
[4] Truong LT, Larsen Å, Holme B, Hansen FK, Roots J. Polymer 2011;52(4): 1116–23.
[5] Goffin AL, Raquez JM, Duquesne E, Siqueira G, Habibi Y, Dufresne A, et al. Polymer 2011;52(4):1532–8.
[6] Potts JR, Dreyer DR, Bielawski CW, Ruof S. Polymer 2011;52(1):5–25.
[7] Rousseaux DDJ, Sallem-Idrissi N, Baudouin A, Devaux J, Godard P, Marchand-Brynaert J, et al. Polymer 2011;52(2):443–51.
[8] Okutan E, Aydin GO, Haciveliogluf F, Kiliç A, Beyaz SK, Yesilot S. Polymer 2011; 52(5):1241–8.
[9] Ajayan PM, Stephan O, Colliex C, Trauth D. Science 1994;265(5176):1212–4.
[10] Ajayan PM, Schadler LS, Giannaris C, Rubio A. Adv Mater 2000;12(10):750–3.
[11] Dalton AB, Collins S, Munoz E, Razal JM, Ebron VH, Ferraris JP, et al. Nature 2003;423(6941):703.
[12] Yoon JT, Lee SC, Jeong YG. Compos Sci Technol 2010;70(5):776–82.
[13] Shieh YT, Liu GL, Twu YK, Wang TL, Yang CH. J Polym Sci Part B Polym Phys 2010;48(2):145–52.
[14] Yuzay IE, Auras R, Soto-Valdez H, Selke S. Polym Degrad Stab 2010;95(9): 1769–77.
[15] Wu DF, Wu L, Zhou WD, Sun YR, Zhang MJ. Polym Sci Part B Polym Phys 2010; 48(4):479–89.
[16] Zeng HL, Gao C, Yan DY. Adv Funct Mater 2006;16(6):812–8.
[17] Thomassin JM, Lou X, Pagnoulle C, Saib A, Bednarz L, Huynen I, et al. J Phys Chem C 2007;111(30):11186–92.
[18] Wu D, Zhang Y, Zhang M, Yu W. Biomacromolecules 2009;10(2):417–24.
[19] Song L, Qiu Z. Polym Degrad Stab 2009;94(4):632–7.
[20] Shih YF, Chen LS, Jeng RJ. Polymer 2008;49(21):4602–11.
[21] González-Vidal N, de Ilarduya AM, Muñoz-Guerra S, Castell P, Martínez MT. Compos Sci Technol 2010;70(5):789–96.
[22] Pramoda KP, Linh NTT, Zhang C, Liu T. J Appl Polym Sci 2009;111(6):2938–45.
[23] Song L, Qiu ZJ. Nanosci Nanotechnol 2010;10(12):965–72.
[24] Wang SF, Shen L, Zhang WD, Tong YJ. Biomacromolecules 2005;6(6):3067–72.
[25] Tasis D, Tagmatarchis N, Bianco A, Prato M. Chem Rev 2006;106(3):1105–36.
[26] Hirsch A. Angew Chem Int Ed Engl 2002;41(11):1853–9.
[27] Kathi J, Rhee KY. J Mater Sci 2008;43(1):33–7.
[28] Tan LC, Chen YW, Zhou WH, Nie HR, Li F, He XH. Polym Degrad Stab 2010; 95(9):1920–7.
[29] Mawhinney DB, Naumenko V, Kuznetsova A, Yates JT, Liu J, Smalley RE. J Am Chem Soc 2000;122(10):2383–4.
[30] Pasternack RM, Amy SR, Chabal YJ. Langmuir 2008;24(22):12963–71.
[31] Oki A, Adams L, Khabashesku V, Edigin Y, Biney P, Luo ZP. Mater Lett 2008; 62(6–7):918–22.
[32] Tang CY, Xiang LX, Su JX, Wang K, Yang CY, Zhang Q, et al. J Phys Chem B 2008;112(13):3876–81.
[33] Kulinski Z, Piorkowska E. Polymer 2005;46(23):10290–300.
[34] Avrami MJ. Chem Phys 1940;8(2):212–24.